Electronic Supplementary Information (ESI)

One-step synthesis of cyclic compounds towards easy room-temperature phosphorescence and deep blue thermally activated delayed fluorescence

Yingyuan Hu,† Zhenfeng Wang,† Xiaofang Jiang, Xinyi Cai, Shi-Jian Su,* Fei Huang* and Yong Cao

Contents

1. General Procedures

General Details.

^{1}H and ^{13}C NMR spectra were measured on a Bruker NMR spectrometer operating at 500 and 126 MHz, respectively, using tetramethylsilane (TMS) as the internal standard. Chemical shifts were expressed in parts per million (ppm), and splitting patterns are designated as s (singlet), d (doublet) and m (multiplet). LC-MS data was obtained on a Bruker Esquire HCT PLUS with atmospheric pressure chemical ionization resource (APCI). MALDI-TOF-MS was measured using a Bruker BIFLEXIII. Thermogravimetric analyses (TGA) were conducted on a NETZSCH TG 209 under a heating rate of 10 °C min^{-1} and a N_2 flow rate of 20 mL min^{-1}. Differential scanning calorimetry (DSC) measurements were operated on a NETZSCH DSC 209 under a N_2 flow at a heating rate of 10 °C min^{-1} and a cooling rate of 20 °C min^{-1}. Cyclic voltammetry data of the compounds in neat film were measured on a CHI600D electrochemical workstation with the scan rate of 50 mV s^{-1} by using Bu_4NPF_6 (0.1 M) in acetonitrile as electrolyte and platinum and saturated calomel electrode as the working and reference electrode, respectively. Elemental analyses were performed on a Vario EL elemental analysis instrument (Elementar Co.).

Optical characterization.

The UV–vis absorption spectra of the compounds were measured on a HP 8453 spectrophotometer over the range of 250–550 nm. Photoluminescence spectra at room temperature and 77 K were recorded on a Jobin Yvon spectro fluorometer equipped with a liquid nitrogen attachment. PL quantum efficiency was measured using an absolute PL quantum yield measurement system (C11347-01, Hamamatsu Photonics) under air at an excitation wavelength of 365 nm. The transient photoluminescence decay characteristics of samples were measured using an output at a central wavelength of 365 nm with a pulse duration of 120 fs and a repetition rate of 20 Hz as the excitation source, which was generated from an optical parametric amplifier (TOPAS-Prime) pumped by a mode-locked Ti:sapphire oscillator seeded regenerative amplifier (SpectraPhysics Spitfire Ace). The laser beam was focused onto the samples using a lens with a focal length of 100 mm. The sample was placed in a cryogenic equipment including an optical vacuum shroud (Janis, 350–10 K closed-cycle refrigerator system). The emission was collected at

the direction perpendicular to the excitation beam to minimize the scattering. The emission signal was directed into a monochromator with two exit ports (Princeton Instruments, Acton 2300i). One port was integrated with a CCD (Princeton Instruments, Pixis 100B) for spectra measurement. The other port was mounted with a photon-counting detector combined with the multichannel scaler/averager SR430 for time-resolved emission measurement. A 395 nm long-pass filter was placed before the spectrometer to minimize the scattering from the excitation light. The emission decay curves from 0 to 100 ns were used to determine τ_p, which were well fitted by a double exponential function. The emission decay curves from 0 to 42 ms were separated using a multiexponential fitting model to determine the contribution from TADF or phosphorescence to the emission. The average lifetime (τ_{av}) was calculated using $\tau_{av} = \Sigma A_i\tau_i^2/\Sigma A_i\tau_i$, where A_i is the pre-exponential factor for lifetime τ_i.

Synthesis and Characterization.

All reagents, unless otherwise specified, were obtained from Alfa Aesar or Sigma-Aldrich and used without further purification. Di(3-bromophenyl)sulfone could be bought from reagent companies or synthesized from the following synthetic steps.

Di(3-bromophenyl)sulfone： To a solution of diphenylsulfone (10.9 g, 50.0 mmol) in H_2SO_4 (50 mL) was added N-bromosuccnimide (17.8 g, 100 mmol) in fractions. The reaction mixture was stirred at 100 °C for 2 h, the resulting mixture was cooled to room temperature and then poured into ice-water (100 mL). The white precipitate was filtered and dried. The crude product was recrystallized from ethanol to produce a white crystal (yield = 11.1 g, 58.8%). ^{1}H NMR (500 MHz, $CDCl_3$): δ 8.08 (t, J = 1.8 Hz, 2H), 7.87 (d, J = 7.9 Hz, 2H), 7.72 (d, J = 8.0 Hz, 2H), 7.41 (t, J = 7.9 Hz, 2H). ^{13}C NMR (126 MHz, $CDCl_3$): δ 143.19, 131.89, 131.75, 127.12, 125.26, 122.70. LC-MS (m/z): $[M+H]^+$ calculated for $C_{12}H_8Br_2O_2S$, 376.06; found, 377.3.

DPTBCO: A catalyst consisting of tris(dibenzylideneacetone)-dipalladium(0) (Pd_2dba_3) (114.46 mg, 0.125 mmol) and tris(*tert*-butyl)phosphine (758.7 μL, 0.75 mmol) dissolved in 20 mL toluene and performed by stirring for 15 min at room temperature was added to di(3-bromophenyl)sulfone (1.8805 g, 5 mmol), aniline (456 μL, 5 mmol), and sodium *tert*-butoxide (1.4415 g, 15 mmol) dissolved in 20 mL toluene. This mixture was stirred for 24 h at 90 °C and then cooled to room

temperature, filtered off, and washed with CH_2Cl_2. After removing the CH_2Cl_2 solvent, the residue was further dissolved in THF. White precipitate was generated and filtered off. After dried in vacuum oven and further sublimated, DPTBCO was obtained as a pale yellow solid (yield = 161.4 mg, 10.5%). ^{1}H NMR (500 MHz, $CDCl_3$): δ 7.70–7.61 (m, 8H), 7.42 (t, *J* = 7.9 Hz, 4H), 7.31 (dd, *J* = 8.3 Hz, 7.5 Hz, 4H), 7.16 (ddd, *J* = 11.3 Hz, 5.7 Hz, 4.7 Hz, 6H), 7.07–7.02 (m, 4H). ^{13}C NMR (126 MHz, $CDCl_3$): due to the poor solubility, the NMR signal was not observed. MALDI-TOF-MS (m/z): $[M]^+$ calculated for $C_{36}H_{26}N_2O_4S_2$, 614.73; found, 614.103; $[M+Na]^+$ calculated for $C_{36}H_{26}N_2O_4S_2$+Na, 637.73; found, 637.085; $[M+K]^+$ calculated for $C_{36}H_{26}N_2O_4S_2$+K, 653.73; found, 653.045. Anal. calcd (%) for $C_{36}H_{26}N_2O_4S_2$: C 70.34, H 4.26, N 4.56, S 10.43; found: C 70.47, H 4.175, N 4.69, S 10.614.

BPTBCO: BPTBCO was synthesized according to a similar procedure as described above for the synthesis of DPTBCO, except that 4-(*tert*-butyl)aniline (796.4 μL, 5 mmol) was used as the reactant instead of aniline, yielding a pale yellow solid (yield = 181.7 mg, 10%). ^{1}H NMR (500 MHz, $CDCl_3$): δ 7.64 (dd, *J* = 7.6 Hz, 1.1 Hz, 8H), 7.41 (t, *J* = 8.1 Hz, 4H), 7.32–7.29 (m, 4H), 7.17–7.13 (m, 4H), 6.97–6.93 (m, 4H), 1.31 (s, 18H). ^{13}C NMR (126 MHz, $CDCl_3$): δ 148.46, 148.37, 143.46, 142.90, 131.06, 128.56, 126.85, 125.36, 122.25, 121.20, 34.49, 31.34. MALDI-TOF-MS (m/z): $[M]^+$ calculated for $C_{44}H_{42}N_2O_4S_2$, 726.95; found, 726.308; $[M+Na]^+$ calculated for $C_{44}H_{42}N_2O_4S_2$+Na, 749.95; found, 749.297; $[M-CH_3]^+$ calculated for $C_{43}H_{39}N_2O_4S_2$, 711.95; found, 711.289. Anal. calcd (%) for $C_{44}H_{42}N_2O_4S_2$: C 72.70, H 5.82, N 3.85, S 8.82; found: C 72.81, H 5.952, N 3.82, S 9.053.

MOPTBCO: MOPTBCO was synthesized according to a similar procedure as described above for the synthesis of DPTBCO, except that 4-methoxyaniline (0.6158 g, 5 mmol) was used as the reactant instead of aniline, yielding a pale yellow solid (yield = 171.9 mg, 10.2%). ^{1}H NMR (500 MHz, $CDCl_3$): δ 7.67 (t, *J* = 2.0 Hz, 4H), 7.62 (ddd, *J* = 7.8 Hz, 1.6 Hz, 0.9 Hz, 4H), 7.40 (t, *J* = 8.0 Hz, 4H), 7.07 (ddd, *J* = 8.2 Hz, 2.3 Hz, 0.8 Hz, 4H), 7.02–6.98 (m, 4H), 6.88–6.85 (m, 4H), 3.81 (s, 6H). ^{13}C NMR (126 MHz, $CDCl_3$): δ 157.43, 148.65, 142.88, 139.04, 131.10, 128.13, 127.86, 122.02, 120.75, 115.36, 55.53. MALDI-TOF-MS (m/z): $[M]^+$ calculated for $C_{38}H_{30}N_2O_6S_2$, 674.79; found, 674.136; $[M+Na]^+$ calculated for $C_{38}H_{30}N_2O_6S_2$+Na, 697.79; found, 697.135. Anal. calcd (%) for $C_{38}H_{30}N_2O_6S_2$: C 67.64, H 4.48, N 4.15, S 9.50; found: C 67.72, H 4.414, N 4.13, S 9.757.

Single Crystal X-Ray Crystallography

Diffraction data were collected at 293 or 150 K on a XtaLAB AFC12 (RCD3): Kappa single four-circle diffractometer using the ω-scan mode with graphite-monochromator Cu×Kα radiation. (λ = 1.54184 Å) The structure was solved with direct methods using the SHELXTL programs and refined with full-matrix least-squares on F2. Non-hydrogen atoms were refined anisotropically. The positions of hydrogen atoms were calculated and refined isotropically.

Wide-angle grazing incidence X-ray scattering (GIWAXS)

The neat film samples for GIWAXS measurement were deposited on the quartz substrate by as-spun coating. The GIWAXS instrument parameters are as follows: Manufacture: Xenocs, France; Model: Xeuss 2.0; X-ray Source: MetalJet-D2, Excillum; Detector: Pilatus3R 1M, Dectris. The test parameters are as follows: SDD = 225.834 mm; Beam Size = 0.8*0.8 mm^2; Beam Center = (270.099, 1026.4); Pixel Size: 0.172*0.172 mm^2; Wavelength: 0.134144 nm; Exposure Time: 1800s.

Time-dependent density functional theory (TD-DFT) calculations

The Gaussian 09 program was utilized to perform the TD-DFT calculations. The ground state (S0) geometries were obtained from the single crystal structures. The exciton energies of the n-th singlet (Sn) and n-th triplet (Tn) states were obtained on the corresponding ground state structure using the combination of TD-B3LYP/6-31G*. Kohn-Sham frontier orbital analysis and spin density distributions were obtained in order to elucidate the mechanisms of possible singlet-triplet intersystem crossings (ISC). The possible S1 to Tn ISC channels are believed to share part of the same transition orbital compositions, and the energy levels of Tn are considered to lie within the range of E_{S1} ± 0.3 or 0.4 eV. Especially, the major ISC channels are mainly determined based on two elements. Firstly, the ratio of the same transition configuration in S1 and Tn should be large in all the transition orbital compositions. Secondly, the energy gap between S1 and the specific Tn state should be small.

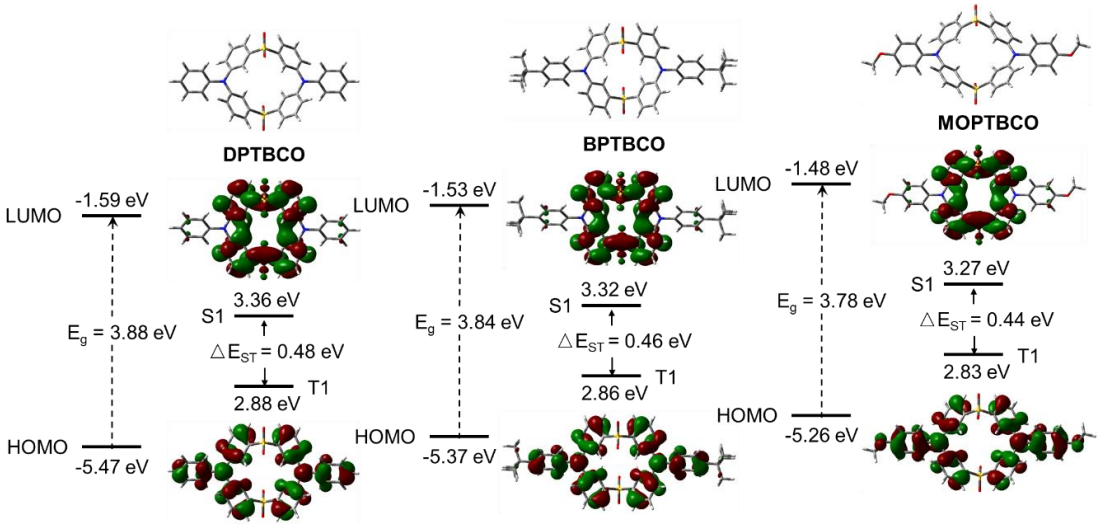

Fig. S1 Molecular structures, HOMO and LUMO distributions, and calculated singlet (S1) and triplet (T1) energy levels for DPTBCO, BPTBCO and MOPTBCO based on TD-DFT at the B3LYP/6-31G(d) level.

2. Thermal & Electrochemical Properties

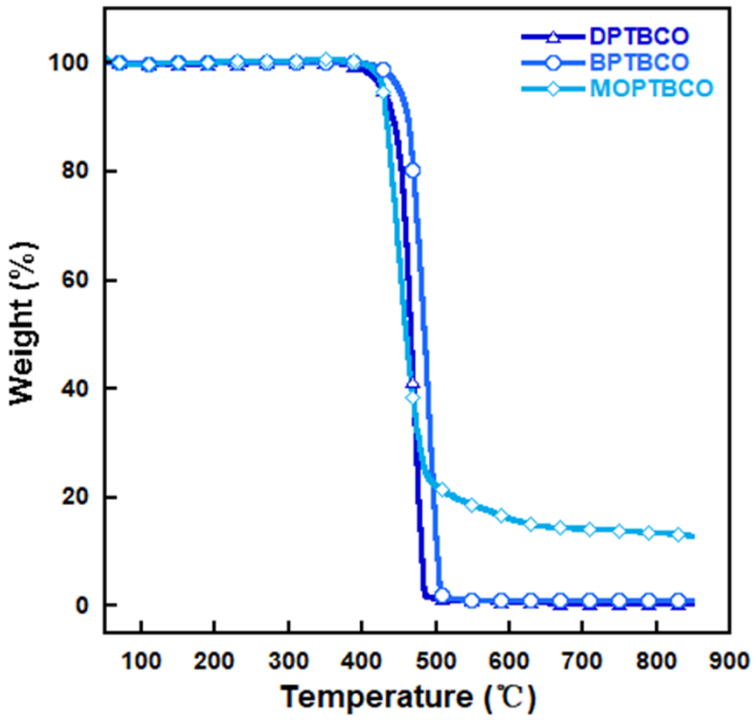

Fig. S2 TGA curves of three compounds at a heating rate of 10 ^{o}C min^{-1} under N_2.

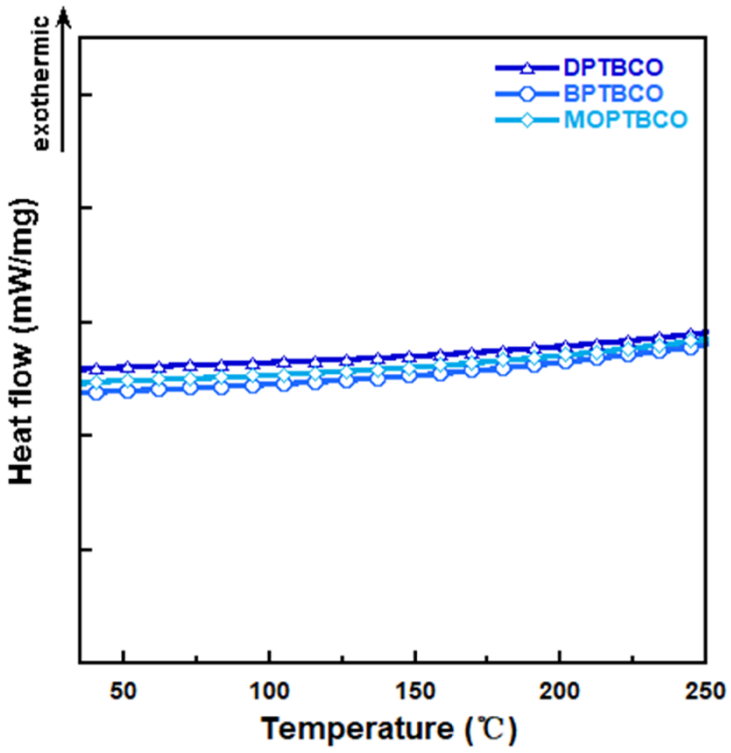

Fig. S3 DSC curves of three compounds recorded during the second heating scan.

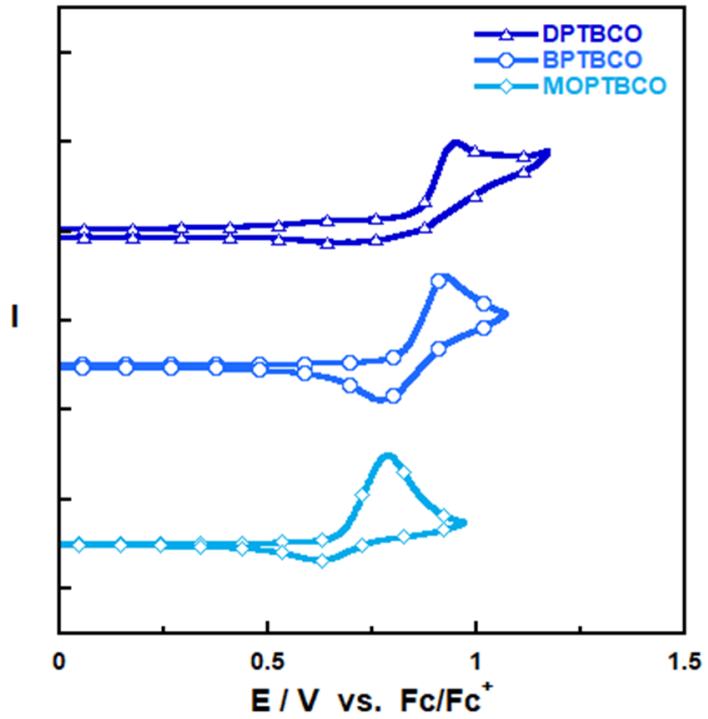

Fig. S4 Cyclic Voltammogram of three compounds.

3. Optical Properties, GIWAXS Measurement, Molecular Stacking and TD-DFT Calculations

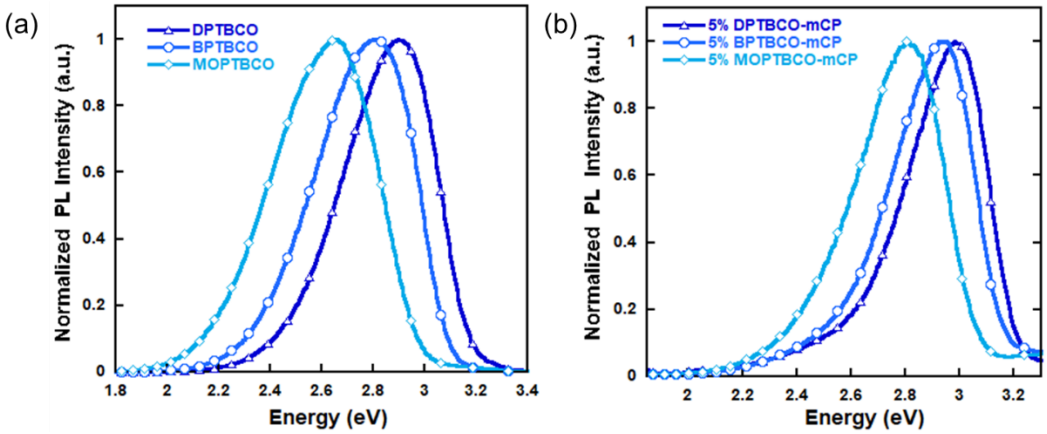

Fig. S5 PL spectra for DPTBCO, BPTBCO and MOPTBCO in DCM solution (a) and in doped films of mCP (5w.t.%) (b).

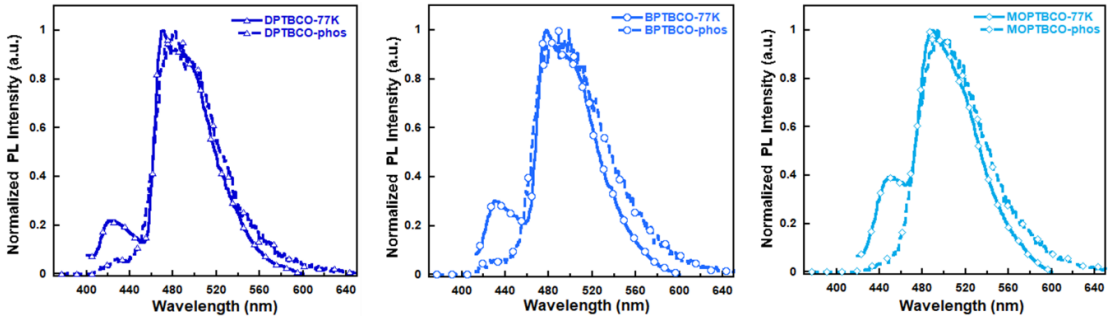

Fig. S6 The low-temperature (77 K) fluorescence and phosphorescence (delayed by 0.2 ms) spectra for three compounds in dichloromethane solutions.

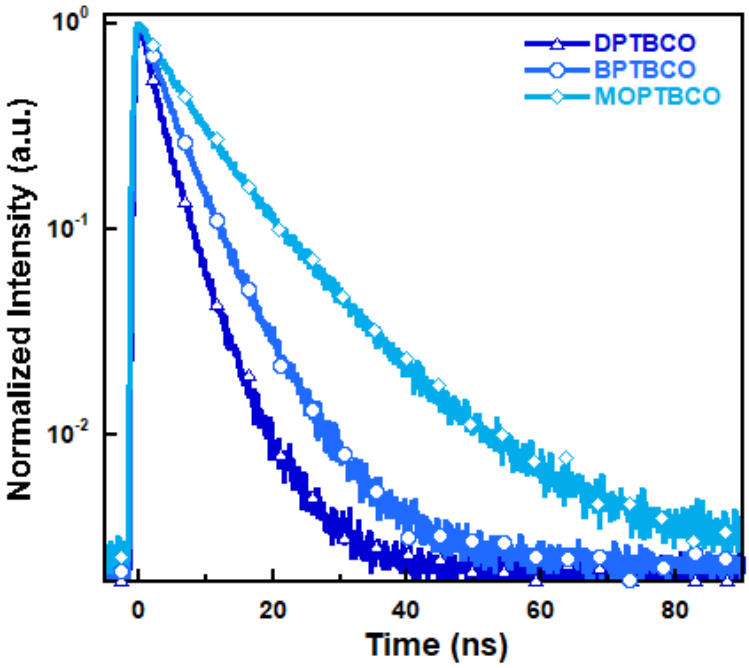

Fig. S7 Prompt emission decay curves of DPTBCO, BPTBCO and MOPTBCO in doped films.

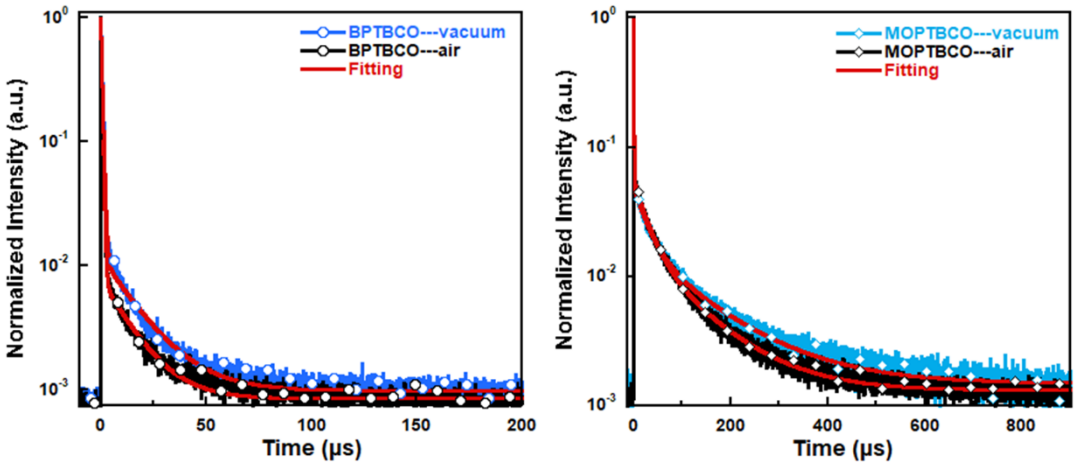

Fig. S8 The comparison of transient PL decays for 5%wt. BPTBCO and MOPTBCO : mCP doped films between in air and under vacuum.

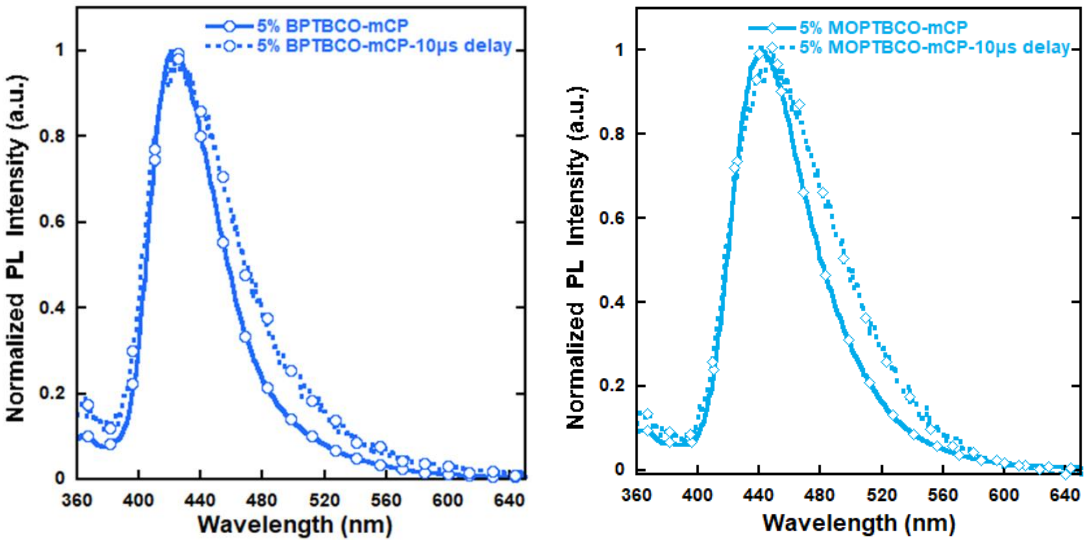

Fig. S9 The photoluminescence spectra of doped films without delay time and 10 μs delay time at room temperature.

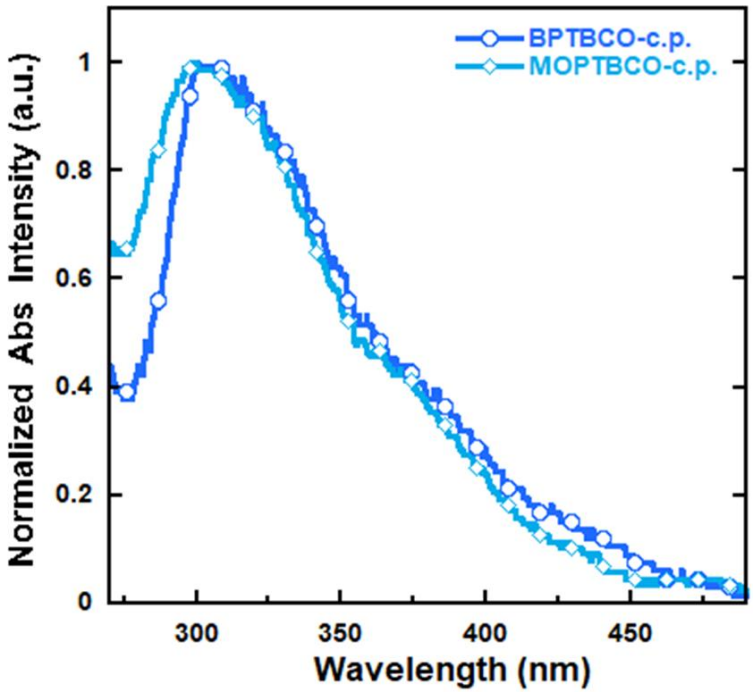

Fig. S10 The absorption spectra of BPTBCO and MOPTBCO in crystalline powder.

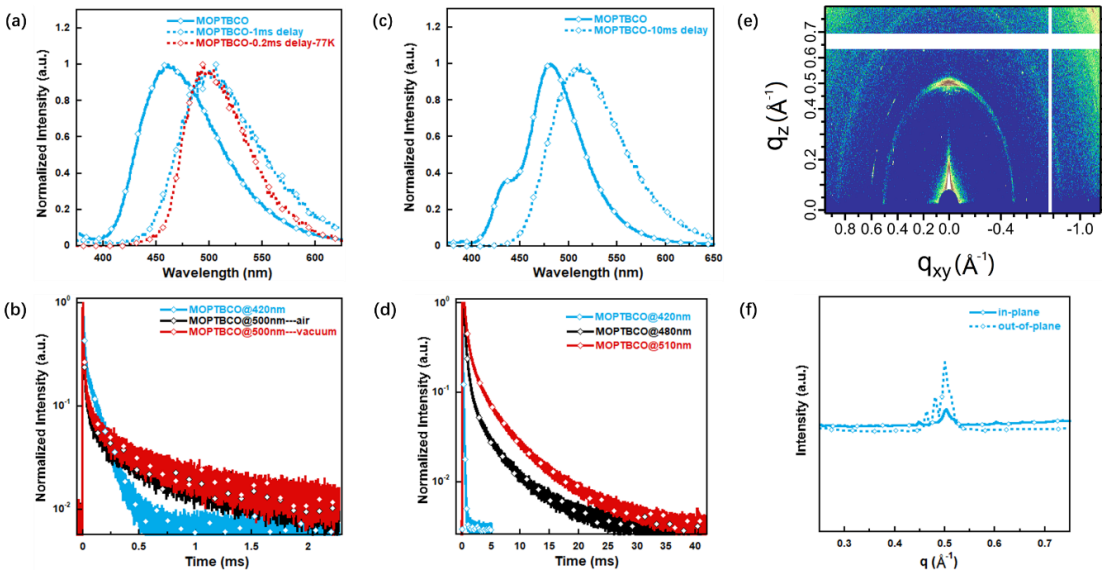

Fig. S11 The steady-state and time-dependent PL spectra for MOPTBCO a) in as-spun neat film and c) in crystal powder. Transient PL decay spectra for MOPTBCO b) in as-spun neat film and d) in crystal powder at different wavelengths at room temperature. e) GIWAXS images of as-spun neat film for MOPTBCO. f) GIWAXS line cuts in the out-of-plane and in-plane direction for MOPTBCO in as-spun neat film.

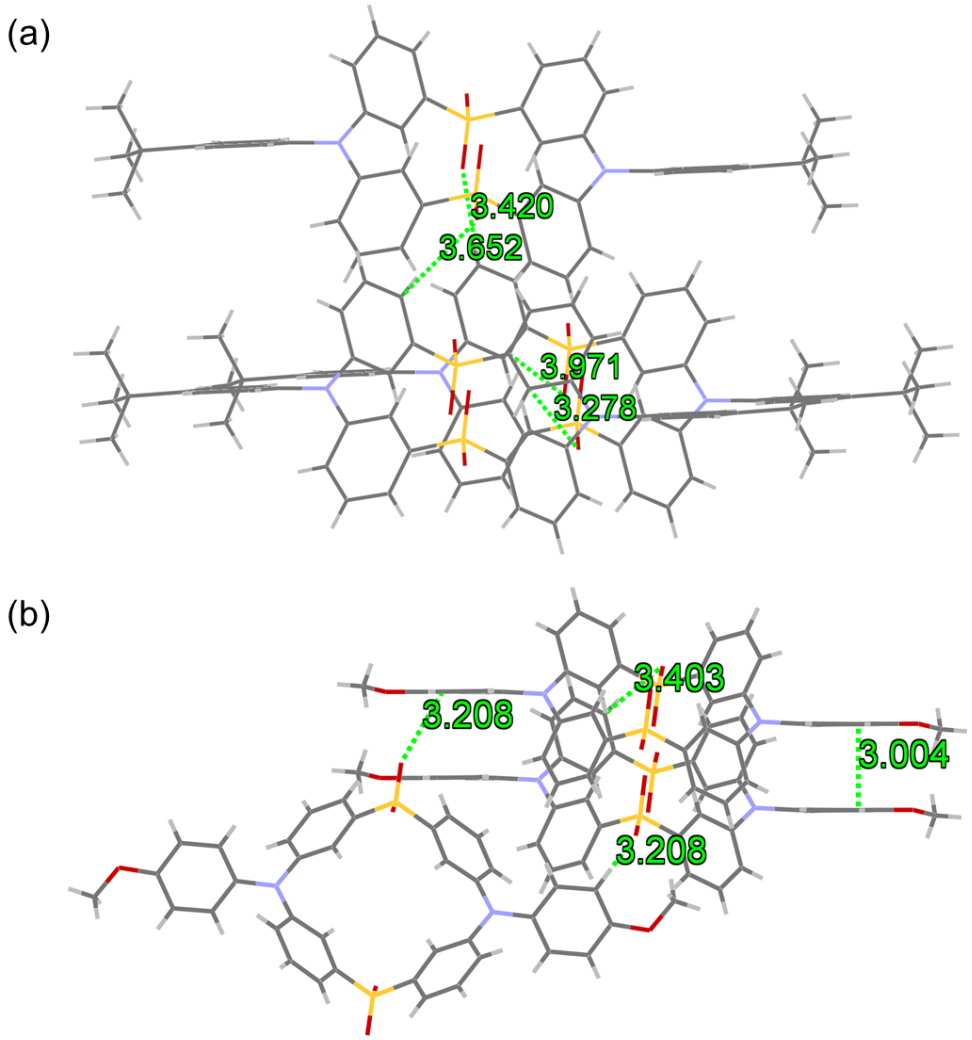

Fig. S12 Intermolecular interactions and molecular packing modes in BPTBCO crystal (a) and MOPTBCO crystal (b).

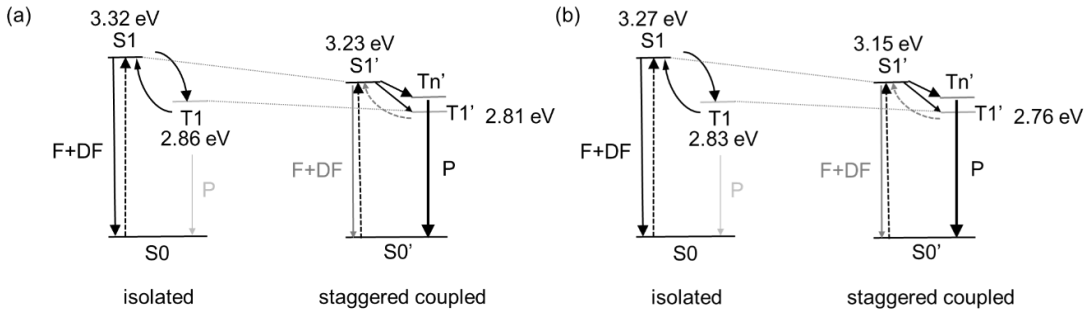

Fig. S13 Energy level schematics of the isolated and coupled BPTBCO molecule(s) (a) and MOPTBCO molecule(s) (b). The color depth of the arrow represents the size of the possibility. F, DF and P refer to fluorescence, delayed fluorescence and phosphorescence, respectively.

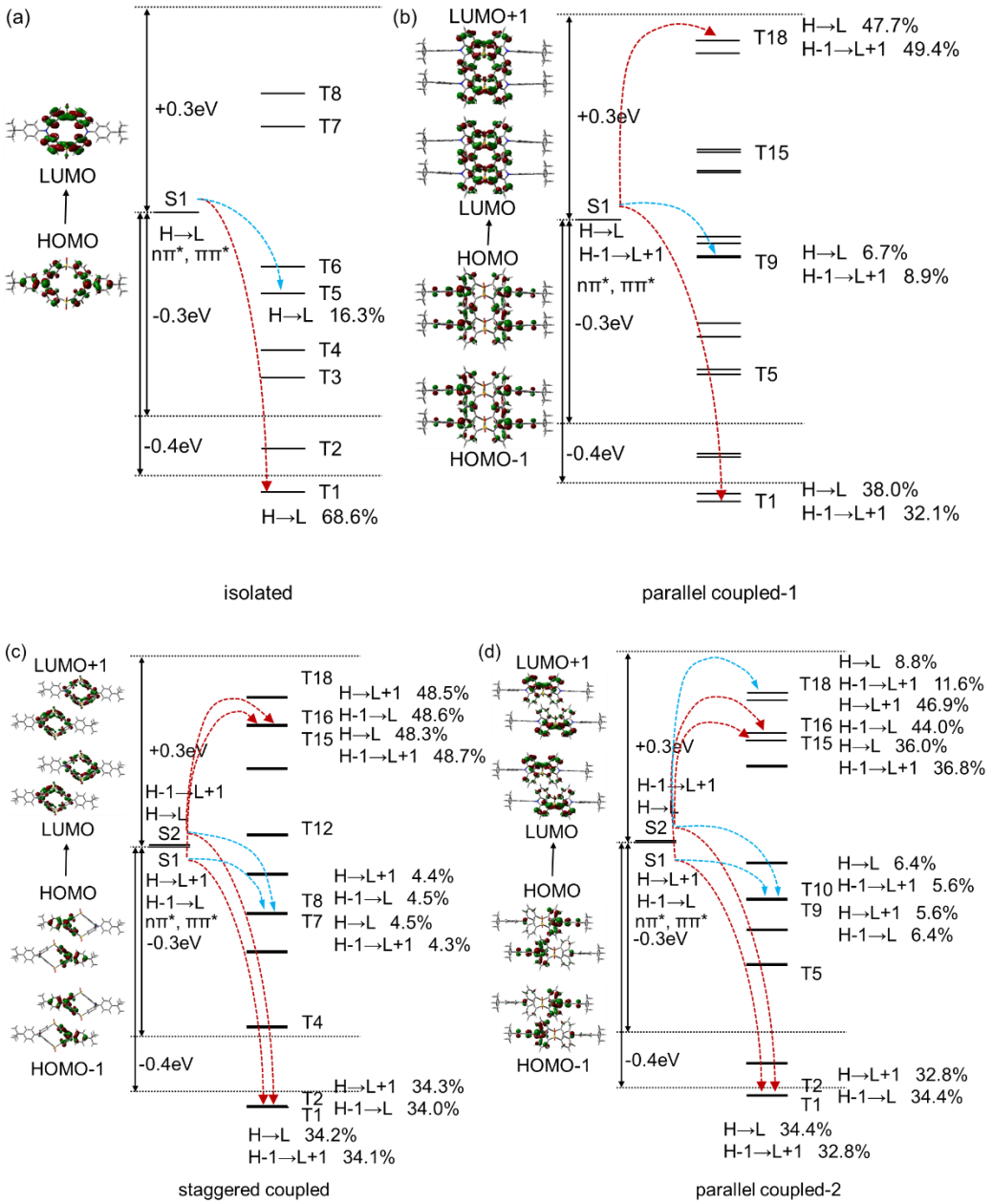

Fig. S14 Schematic representations of the TD-DFT calculated energy levels, main orbital configurations, and possible intramolecular and intermolecular ISC channels of a) isolated BPTBCO, c) staggered coupled BPTBCO and b, d) parallel coupled BPTBCO at the singlet (S1/S2) and triplet (Tn) states. H and L refer to HOMO and LUMO, respectively. The red and blue arrows refer to the relative major and minor ISC channels in a), b), c) and d), respectively.

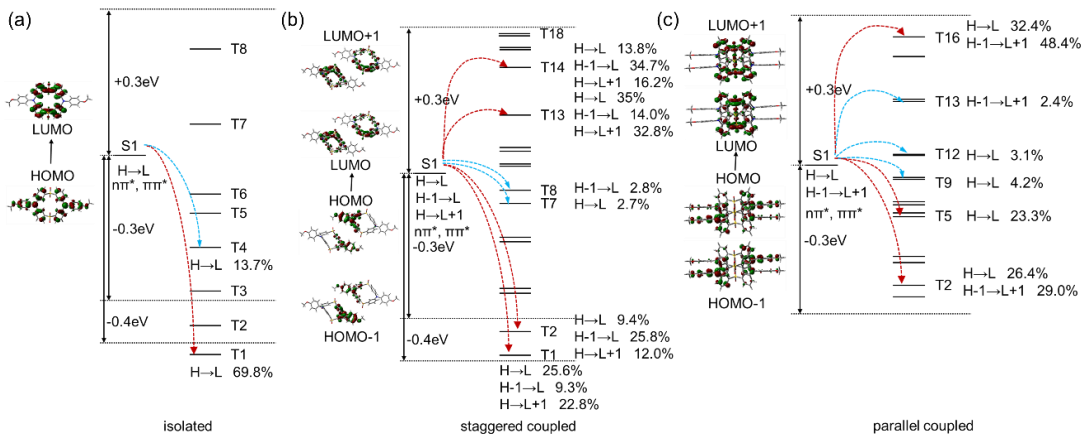

Fig. S15 Schematic representations of the TD-DFT calculated energy levels, main orbital configurations, and possible intramolecular and intermolecular ISC channels of a) isolated MOPTBCO, b) staggered coupled MOPTBCO and c) parallel coupled MOPTBCO at the singlet (S1) and triplet (Tn) states. H and L refer to HOMO and LUMO, respectively. The red and blue arrows refer to the relative major and minor ISC channels in a), b) and c), respectively.

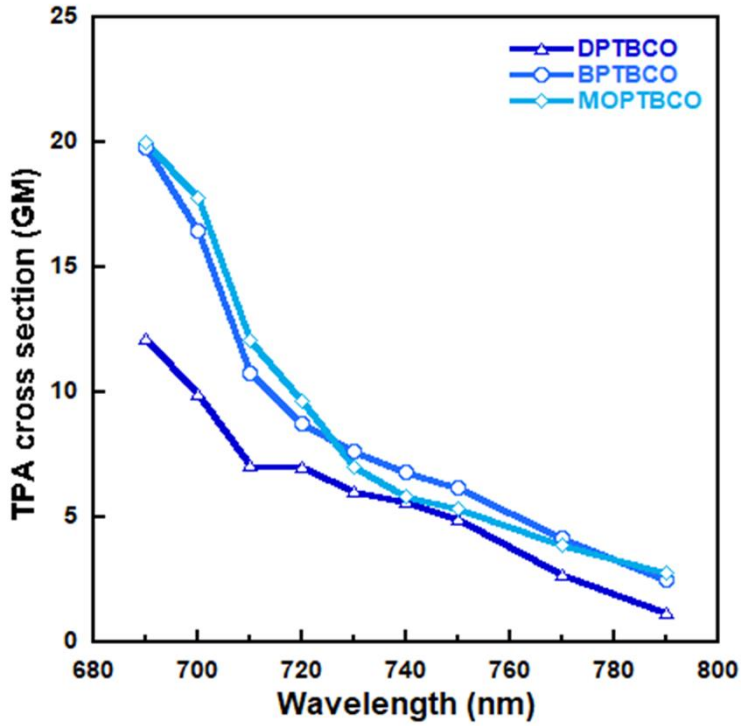

Fig. S16 Wavelength dependent two-photon absorption (TPA) cross section values for three compounds by using Fluorescein in water (pH = 11) as the reference. All three compounds display largest TPA cross sections at 690 nm, the shortest excitation wavelength used in the experiment (the real TPA maximum could be located at even shorter wavelength beyond our measurement window). MOPTBCO shows larger TPA cross section value owing to longer conjugation length resulting from the lone-pair electrons in the methoxy substituents, which is within the normal

range. Two-Photon Excitation (2PE) fluorescence were measured by using an Avesta TiF-100 M femtosecond (fs) Ti:sapphire oscillator as the excitation source. The output laser pulses have pulse duration of 80 fs and a repetition rate of 84.5 MHz in the wavelength range from 690 to 790 nm. The laser beam was focused onto the sample that was contained in a cuvette with path length of 1 cm. The emission was collected at an angle of 90° to the incoming excitation beam by a pair of lenses and an optical fiber that was connected to a monochromator (Acton, Spectra Pro 2300i) coupled CCD (Princeton Instruments, Pixis 100B) system. A short pass filter with cutoff wavelength at 690 nm was placed before the spectrometer to minimize the scattering from the pump beam. Fluorescein in water (pH 11) was used as reference (r). TPA cross section (δ) of the sample (s) at each wavelength can be calculated according to

$$\delta_s = \frac{I_s}{I_r} \cdot \frac{\varphi_r}{\varphi_s} \cdot \frac{C_r}{C_s} \cdot \delta_r$$

where I is the integrated 2PE fluorescence signals, φ is the fluorescence quantum yield, and C is concentration.

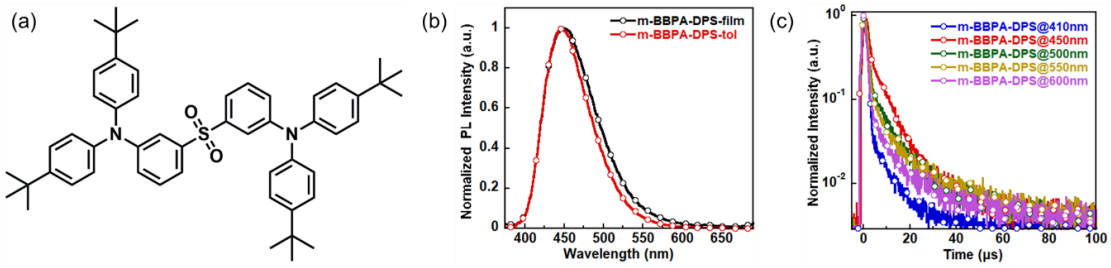

Fig. S17 a) The chemical structure of the non-cyclized molecule m-BBPA-DPS (PLQY: 10.4% in as-spun neat film). A catalyst consisting of tris(dibenzylideneacetone)-dipalladium(0) (Pd_2dba_3) (0.2747 g, 0.3 mmol) and tris(*tert*-butyl)phosphine (1.82 mL, 1.8 mmol) dissolved in 10 mL toluene and preformed by stirring for 15 min at room temperature was added to di(3-bromophenyl)sulfone (1.1283 g, 3 mmol), di-4-*tert*-butylphenylamine (1.6886 g, 6 mmol), and sodium *tert*-butoxide (1.7298 g, 18 mmol) dissolved in 100 mL toluene. This mixture was stirred for 24 h at 90 °C and then cooled to room temperature, filtered off, and washed with CH_2Cl_2. After removing the solvent, the product was purified by chromatography on silica gel (petroleum ether/CH_2Cl_2 = 2:3) and recrystallized from tetrahydrofuran/methanol to obtain the desired pure product (1.94 g, yield: 83%). ^{1}H NMR (500 MHz, $CDCl_3$): δ 7.57 (t, *J* = 1.9 Hz, 2H), 7.32–7.28 (m, 2H), 7.26–7.23 (m, 10H), 7.13 (ddd, *J* = 8.1, 2.3, 1.0 Hz, 2H), 6.98–6.93 (m, 8H), 1.30 (s, 36H). ^{13}C NMR (126 MHz, $CDCl_3$): δ 149.08, 146.84, 144.03, 142.26, 129.71, 126.38, 125.79, 124.37, 120.07, 119.42, 34.36, 31.40. LC-MS (m/z): $[M+H]^+$ calculated for $C_{52}H_{60}N_2O_2S$, 777.12; found, 778.2. b) PL spectra of m-BBPA-DPS in as-spun neat film and in toluene solution. c) Transient PL decay spectra of m-BBPA-DPS in as-

spun neat film at different wavelengths at room temperature. Based on the above measurements, significant differences in optical properties between cyclic and non-cyclized molecules could be observed. For the non-cyclized molecule (m-BBPA-DPS), there is only single emission peak in as-spun neat film, similar with that in toluene, which should come from fluorescence and delayed fluorescence. From the transient PL decay spectra at different wavelengths, it can be seen that the lifetime at the position of the wave peak is the longest one, which implies that there is no room temperature phosphorescence (RTP). In a word, the unique RTP property of cyclic molecules in as-spun neat film is mainly attributed to their specific cyclic structure which makes the molecules more planar and thus promotes orderly accumulation.

4. Table Data

Table S1 Photophysical properties of DPTBCO, BPTBCO and MOPTBCO.

	T_d (°C)	λ_{ab}(nm) sol[a]	λ_{em}(nm) sol[a]/film[b]/ c.p.[c]	HOMO/ LUMO (eV)	τ_p[b] (ns)	τ_d[b] (μs)	τ_{ph}[d] (ms)	Φ[a] (%)	FWHM[e] (nm)	ΔE_{ST}[f] (eV)
DPTBCO	428	298/360	427/416/ 415 470	5.69/2.68	3.78	10.9	/	7.2 (8)	64 (49)	0.34
BPTBCO	450	299/366	443/424/ 432 468	5.63/2.63	5.55	16.1	0.47 (4.55)	9.3 (10.9)	74 (53)	0.31
MOPTBCO	428	295/364	469/441/ 439 481	5.48/2.58	9.97	101.3	0.67 (5.09)	11.4 (14)	89 (61)	0.24

[a] Measured in DCM solution. The values in parentheses are obtained by bubbling N_2 for 3 minutes. [b] Measured in doped film (5w.t.% in mCP). [c] Measured in crystal powder. [d] Measured in as-spun neat film. The values in parentheses are obtained in crystal powder. [e] full-width at half-maximum in DCM solution. The values in parentheses are obtained in doped film. [f] Evaluated in DCM solution at 77 K.

Table S2 Summary of lifetime and delayed component content for DPTBCO, BPTBCO and MOPTBCO in doped films (5 w.t.% in mCP) between in air and under vacuum.

	delay lifetime (μs)		delayed component content (%)	
	air	vacuum	air	vacuum
DPTBCO	7.8	10.9	0.4	10.5
BPTBCO	13.5	16.1	13.5	22
MOPTBCO	76.4	101.3	76.5	80

Table S3 Crystallographic data of BPTBCO and MOPTBCO.

	BPTBCO	MOPTBCO
CCDC	1583478	1583482
Empirical formula	C44 H42 N2 O4 S2	C38 H30 N2 O6 S2
Formula weight	726.91	674.76
Temperature	293(2) K	149.99(10) K
Wavelength	1.54184 Å	1.54184 Å
Crystal system	Triclinic	Monoclinic
Space group	P-1	P 1 21/c 1
a	7.2994(2) Å	13.5501(6) Å
b	9.0319(3) Å	4.9755(2) Å
c	14.3088(3) Å	23.1851(10) Å
α	84.935(2)°.	90°
β	77.163(2)°.	100.243(4)°
γ	84.614(2)°.	90°
Volume	913.49(4) $Å^3$	1538.19(12) $Å^3$
Z	1	2
Density (calculated)	1.321 Mg/m^3	1.457 Mg/m^3
Absorption coefficient	1.695 mm^{-1}	2.021 mm^{-1}
F(000)	384	704
Crystal size	0.21 x 0.2 x 0.19 mm^3	0.21 x 0.2 x 0.19 mm^3
Theta range for data collection	4.930 to 67.072°.	3.314 to 67.063°.
Index ranges	-8<=h<=8, -6<=k<=10, -17<=l<=17	-16<=h<=13, -3<=k<=5, -27<=l<=27
Reflections collected	7076	5881
Independent reflections	3202 [R(int) = 0.0273]	2706 [R(int) = 0.0428]
Completeness to theta = 67.063°	98.00%	99.50%
Absorption correction	n/a	multi-scan
Max. and min. transmission	n/a	1.00000 and 0.66142
Refinement method	Full-matrix least-squares on F^2	Full-matrix least-squares on F^2
Data / restraints / parameters	3202 / 0 / 239	2706 / 0 / 218
Goodness-of-fit on F^2	1.075	1.06
Final R indices [I>2sigma(I)]	R1 = 0.0414, wR2 = 0.1107	R1 = 0.0411, wR2 = 0.1165
R indices (all data)	R1 = 0.0426, wR2 = 0.1114	R1 = 0.0435, wR2 = 0.1190
Extinction coefficient	0.0081(9)	n/a
Hydrogen treatment	constr	constr
Largest diff. peak and hole	0.542 and -0.470 $e.Å^{-3}$	0.286 and -0.416 $e.Å^{-3}$

5. NMR and MS Spectra

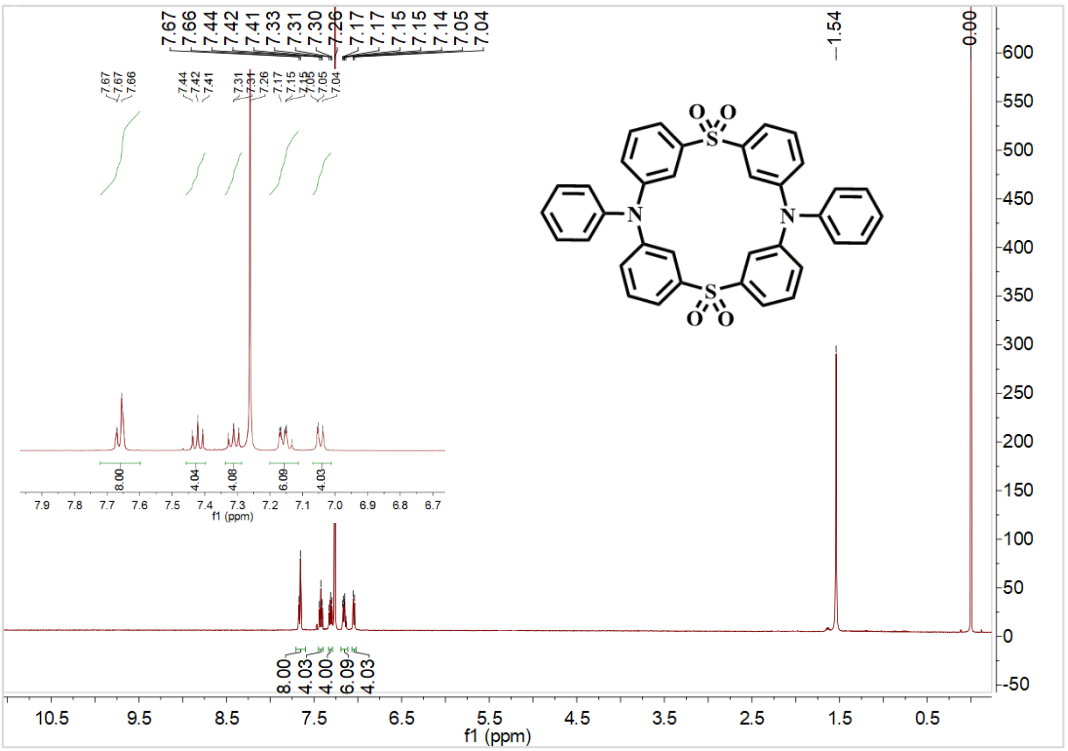

Fig. S17 ^{1}H NMR spectrum of **DPTBCO** in $CDCl_3$.

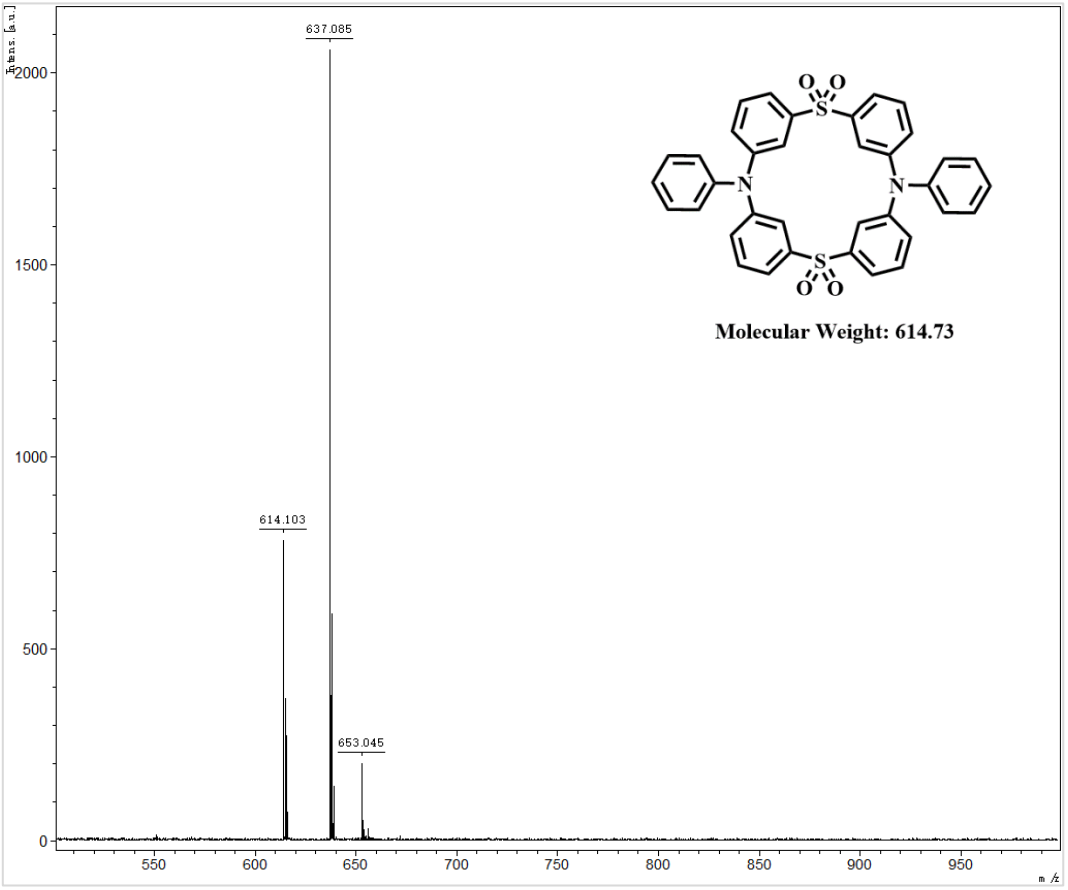

Fig. S18 MALDI-TOF-MS of **DPTBCO**.

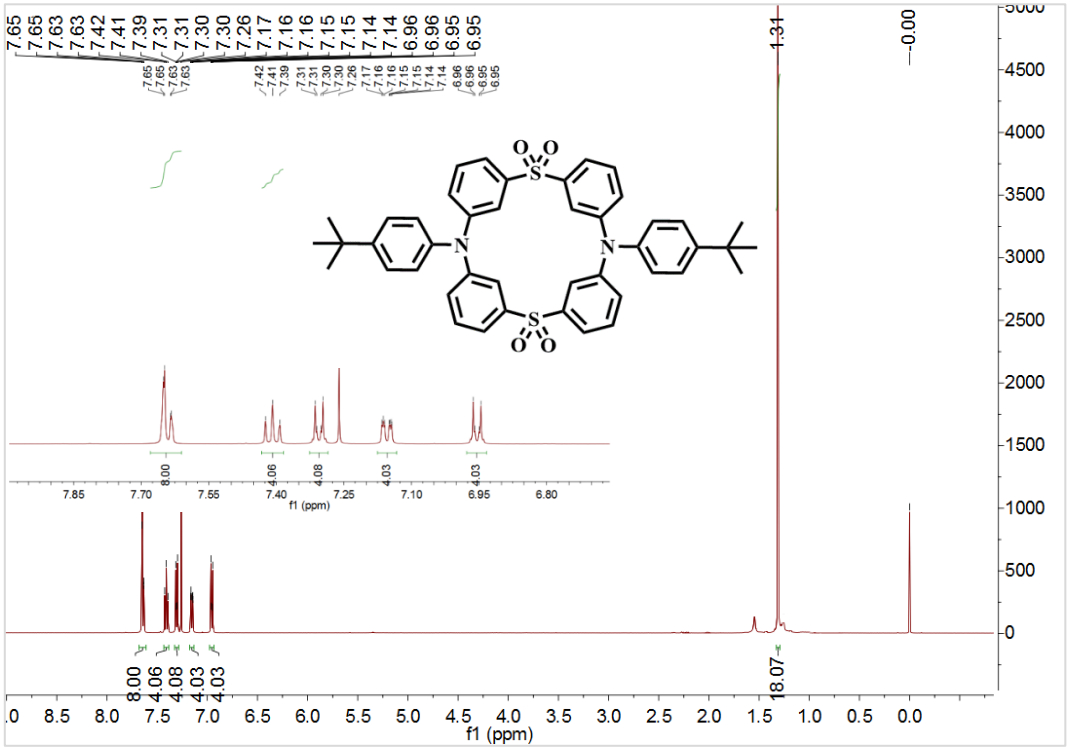

Fig. S19 ^{1}H NMR spectrum of **BPTBCO** in $CDCl_3$.

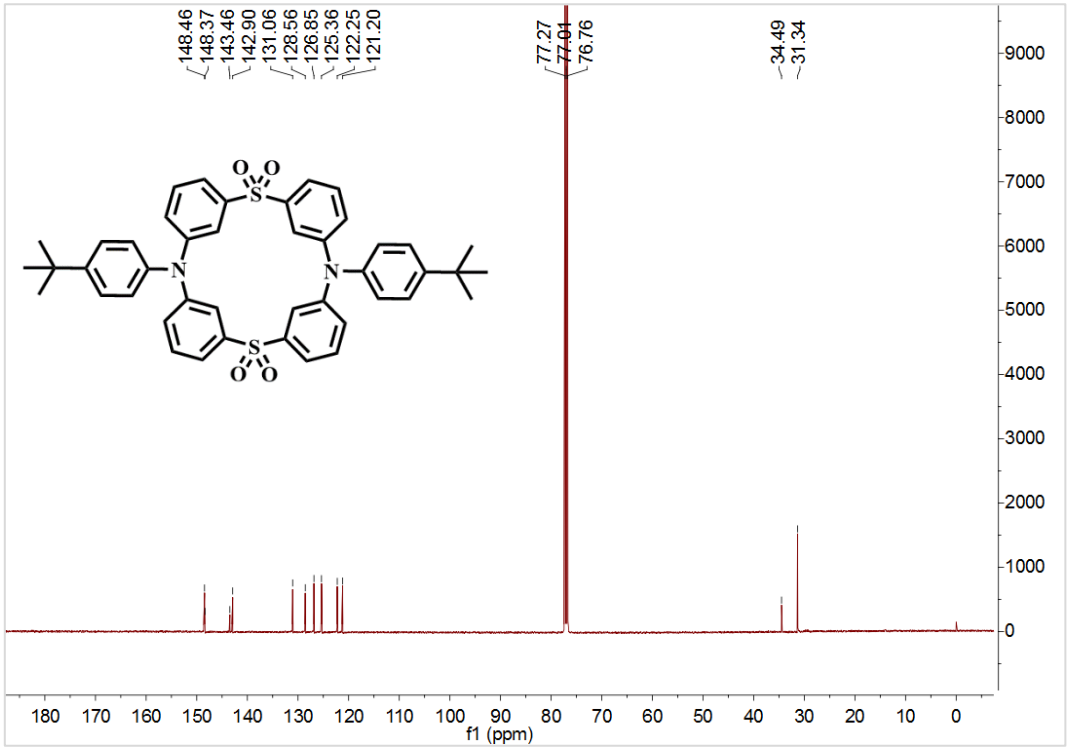

Fig. S20 ^{13}C NMR spectrum of **BPTBCO** in $CDCl_3$.

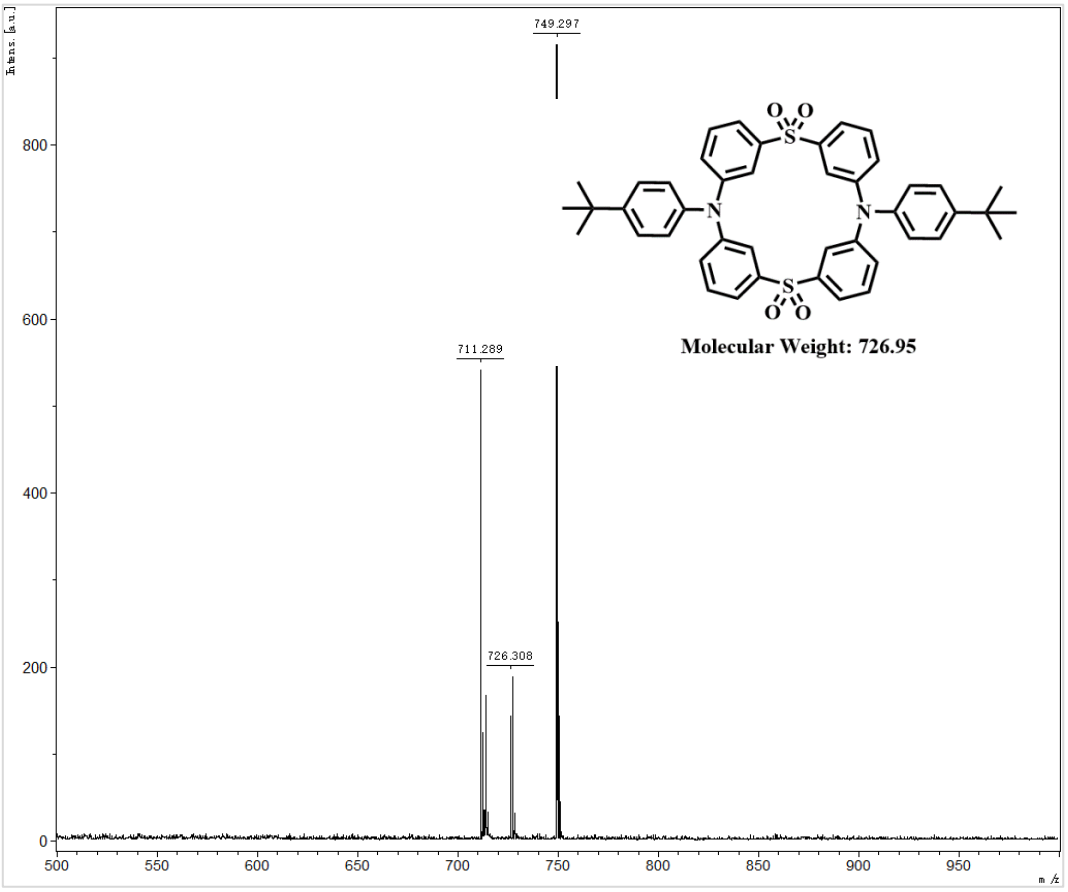

Fig. S21 MALDI-TOF-MS of **BPTBCO**.

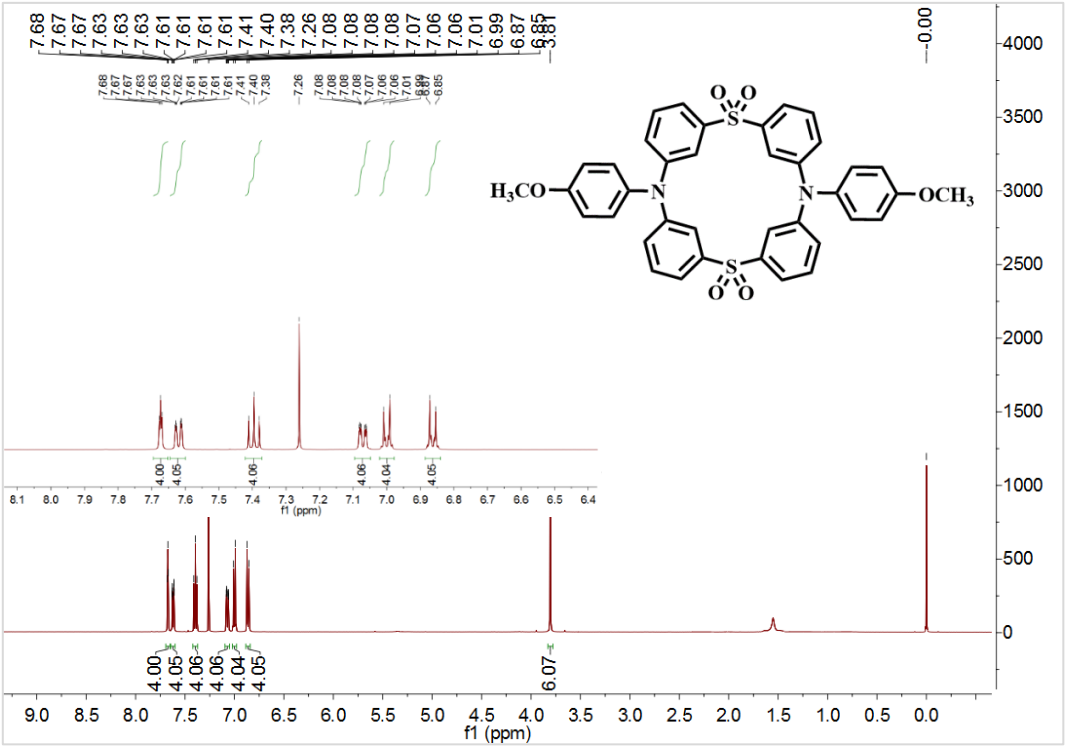

Fig. S22 ^{1}H NMR spectrum of **MOPTBCO** in $CDCl_3$.

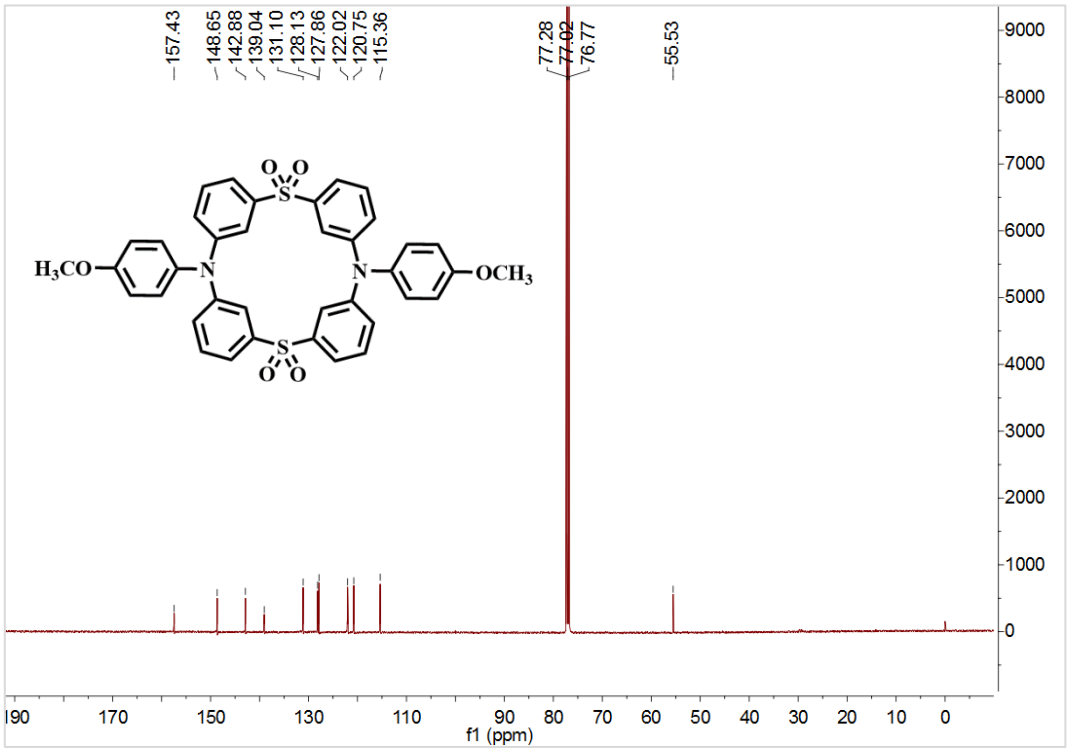

Fig. S23 ^{13}C NMR spectrum of **MOPTBCO** in $CDCl_3$.

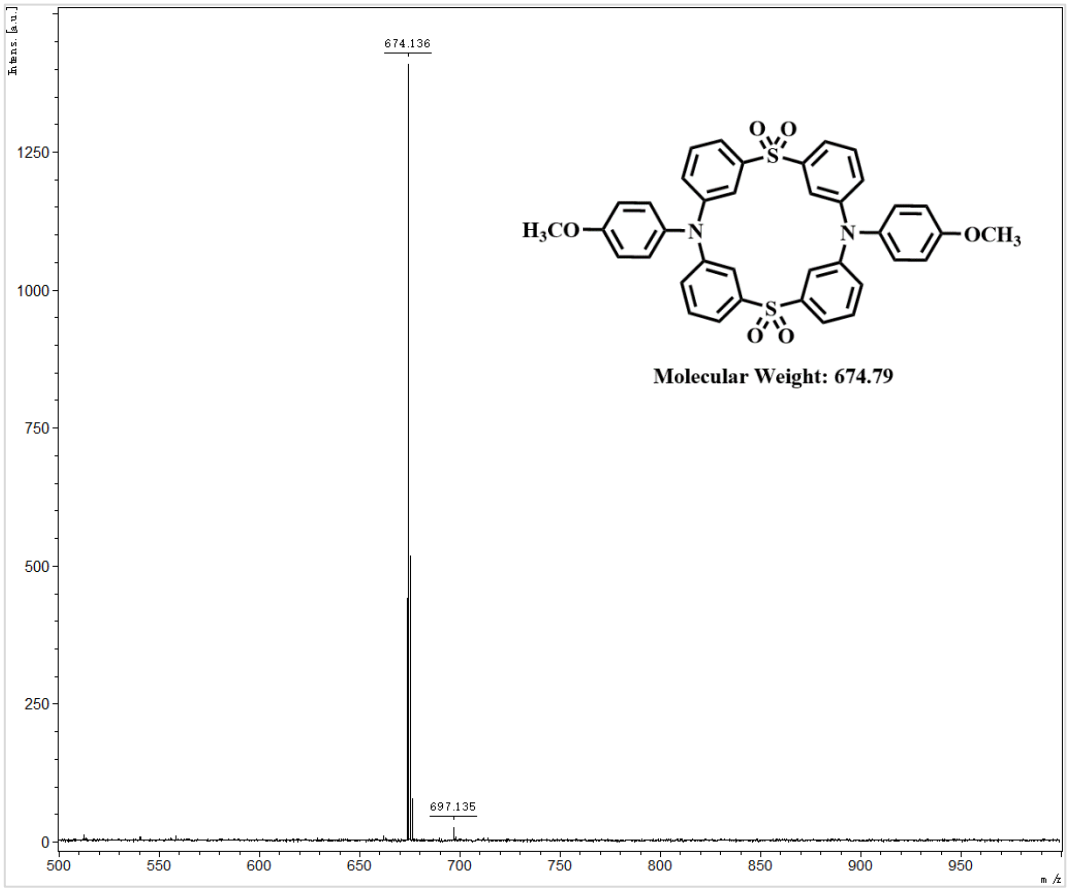

Fig. S24 MALDI-TOF-MS of **MOPTBCO**.